Supplement of Atmos. Chem. Phys., 20, 2953–2966, 2020
https://doi.org/10.5194/acp-20-2953-2020-supplement

Atmospheric Chemistry and Physics
Open Access
EGU

Supplement of

Impact of poleward heat and moisture transports on Arctic clouds and climate simulation

Eun-Hyuk Baek et al.

Correspondence to: Sungsu Park (sungsup@snu.ac.kr) and Baek-Min Kim (baekmin@pknu.ac.kr)

Supplementary Information

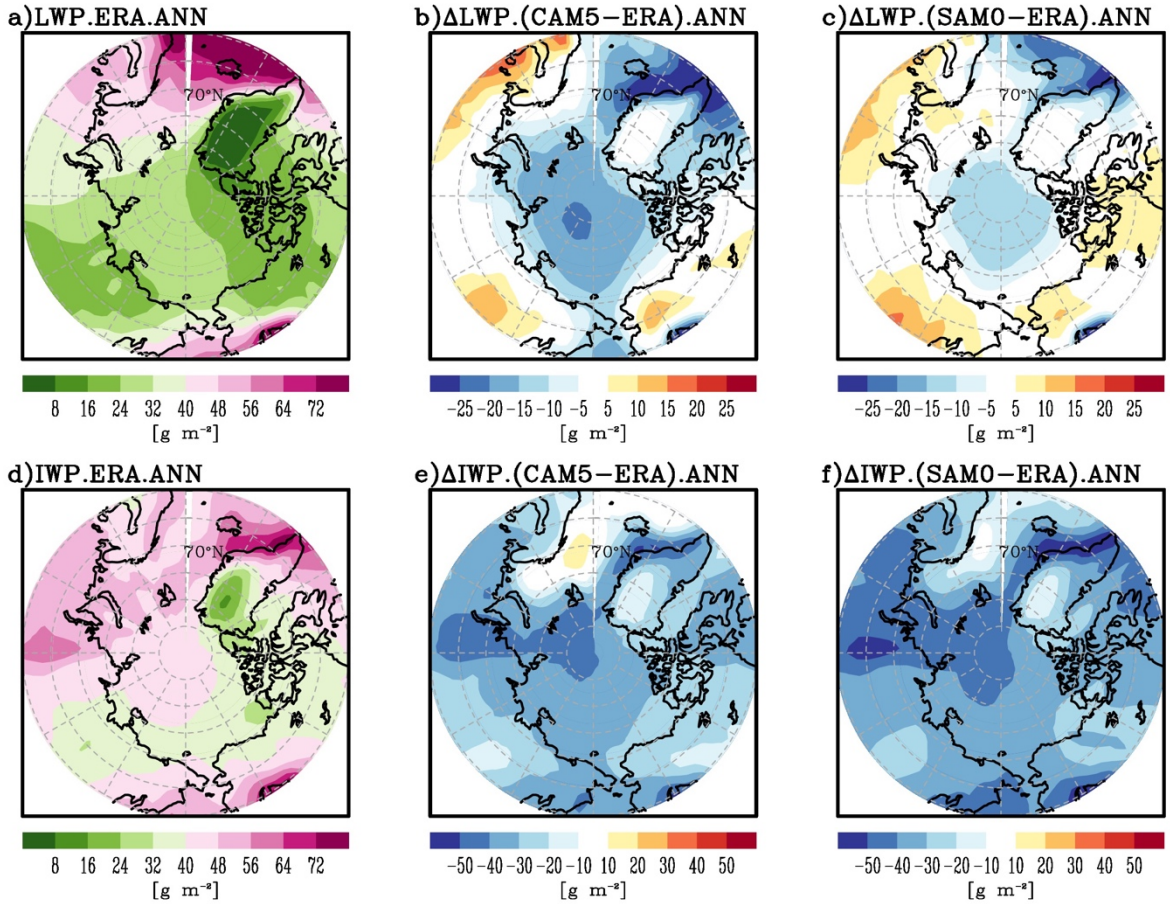

Supplementary Figure S1. Annual mean liquid water path (LWP) (upper panel) and ice water path (IWP) (bottom panel) of ERA interim data (left) and the differences of CAM5 (center) and SAM0 (right) from ERA interim data. ERA-Interim reanalysis was averaged from January 1979 to February 2015 and the model results are the means of AMIP simulation results for 36 years from January 1979 to February 2015.

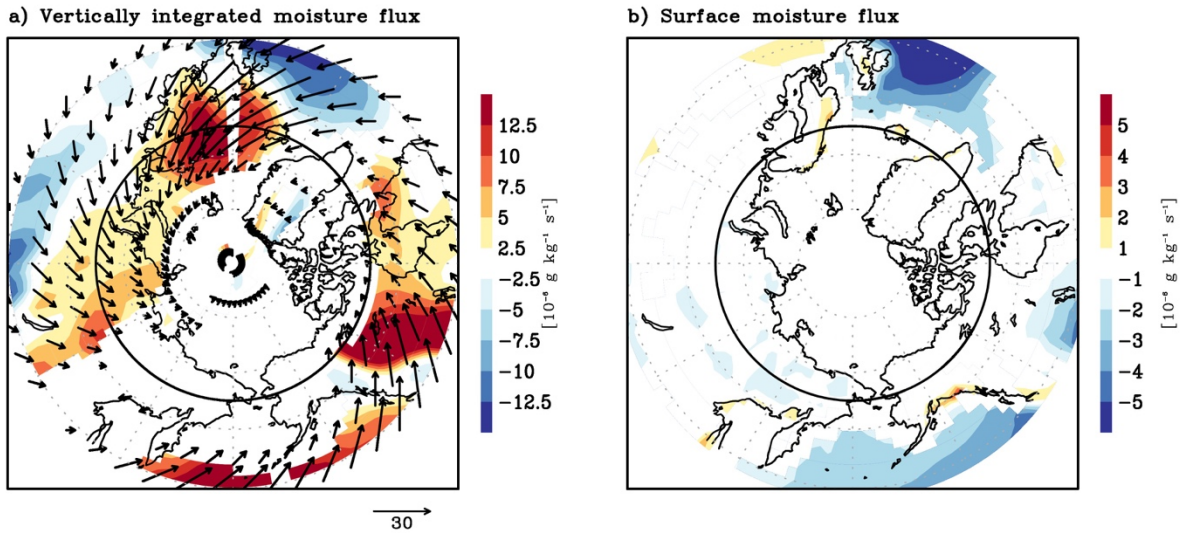

Supplementary Figure S2. Differences of (a) vertically-integrated annual-mean horizontal moisture flux in g kg^{-1} m s^{-1} (arrow) and its convergence in 10^{-6} g kg^{-1} s^{-1} (shaded) and (b) surface moisture flux in 10^{-6} g kg^{-1} s^{-1} between SAM0 and CAM5. Black contour denotes the Arctic circle (65° N). All vectors and shaded areas exceed a 95 % significance level from the Student t-test.

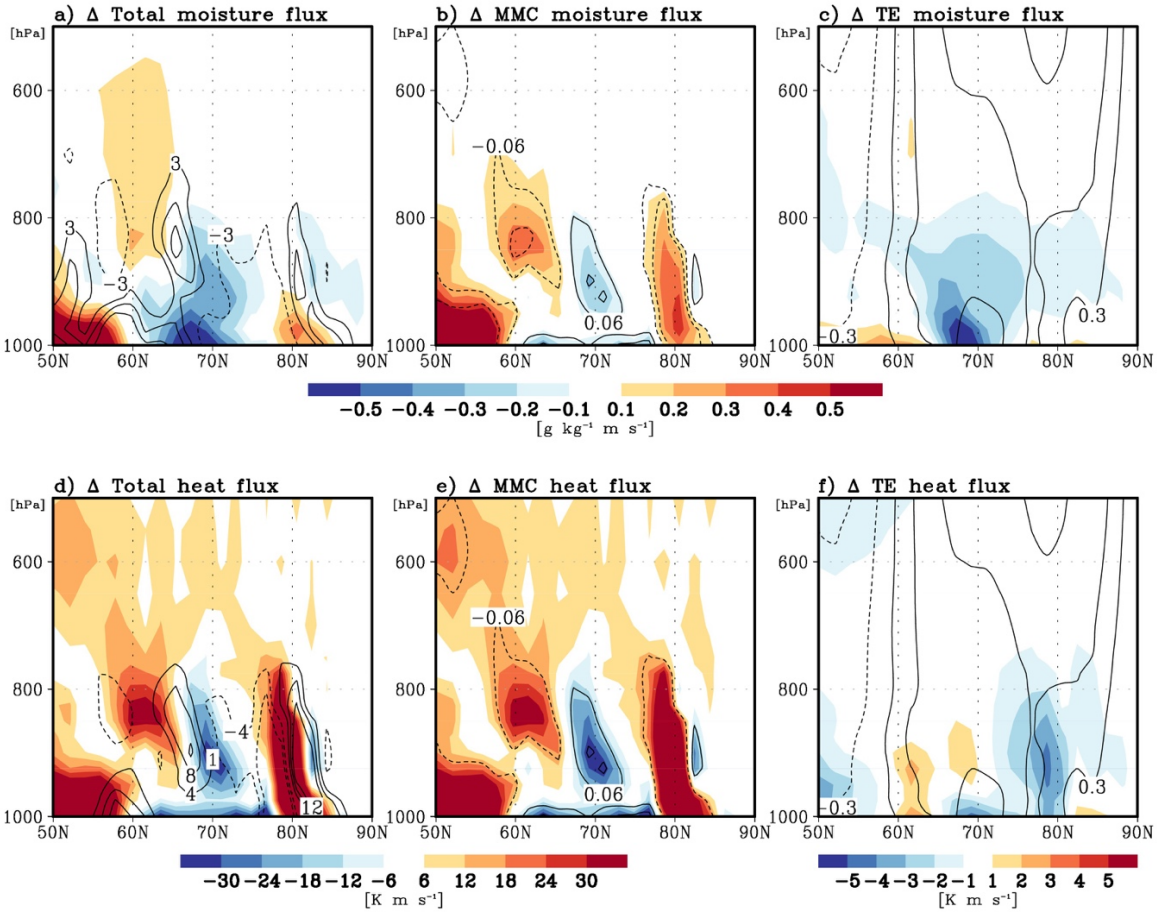

Supplementary Figure S3. CAM5 biases of zonal-mean meridional fluxes of (a, b, and c) moisture and (d, e, and f) heat by (a and d) total processes (i.e., the transported sum by mean meridional circulation, stationary eddies, and transient eddies), (b and e) mean meridional circulation (MMC), and (c and f) transient eddies (TE) against the ERA-interim reanalysis. The black lines in (a) and (d) denote the bias of zonal-mean convergence of total moisture flux in 10^{-7} g kg^{-1} s^{-1} and total heat flux in 10^{-5} K s^{-1}, the black lines in (b) and (e) denote the bias of zonal mean meridional wind in m s^{-1}, and the black lines in (c) and (f) denote the bias of zonal-mean zonal wind in m s^{-1} against the ERA-interim reanalysis, respectively.

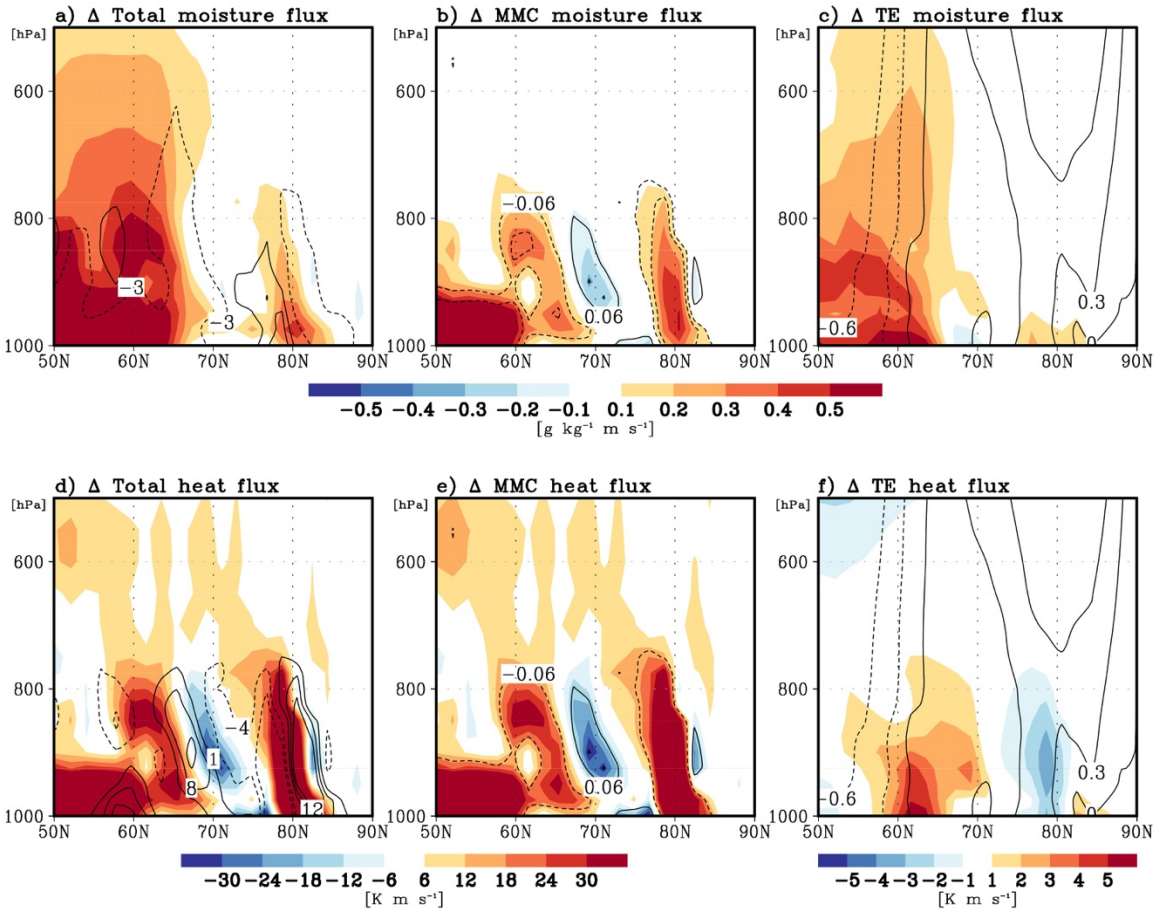

Supplementary Figure S4. Identical with supplementary figure S3 except for SAM0.

30

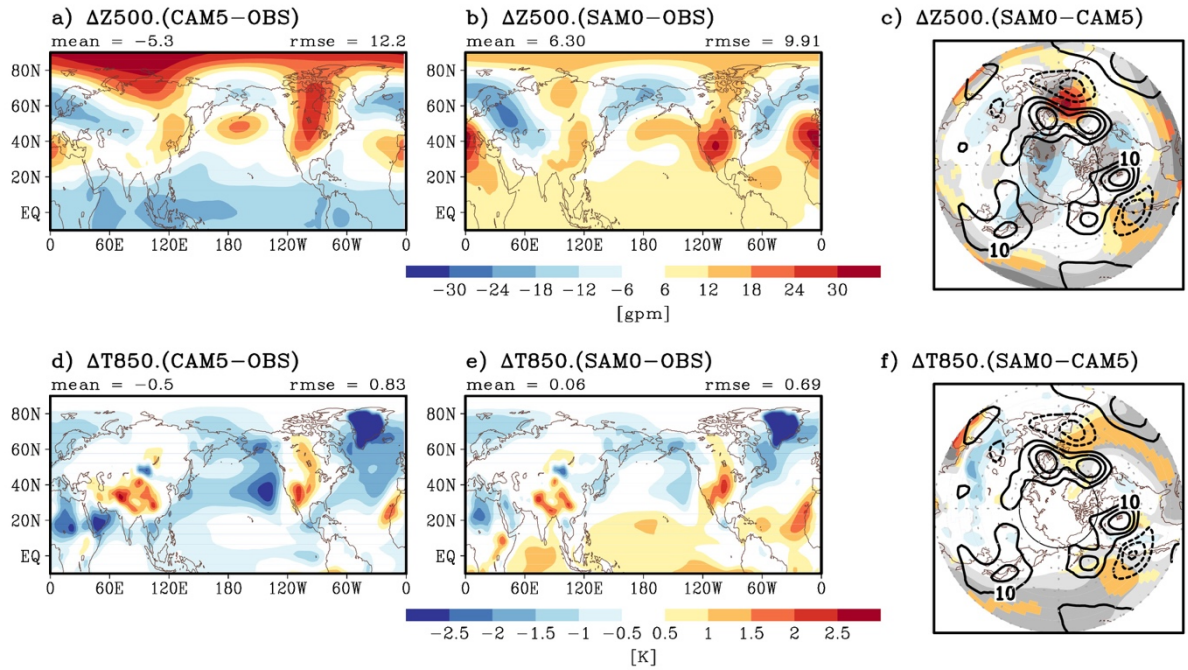

Supplementary Figure S5. Differences of annual-mean (upper) 500 hPa geopotential height (Z500) and (lower) 850 hPa air temperature (T850) between (left) CAM5 and ERA-interim reanalysis observation, (center) SAM0 and observation, and (right) SAM0 and CAM5. ERA-Interim reanalysis was averaged from January 1979 to February 2015 and the model results are the means of AMIP simulation results for 36 years from January 1979 to February 2015. The thick black contours in (c) and (f) denote the difference of storm track activity at 300 hPa defined as the transient meridional velocity variance (v'v') and thin black contours denote the Arctic circle (65° N). Color shaded and contoured areas in (c), (f), and (i) exceed a 95 % significance level from the Student t-test.

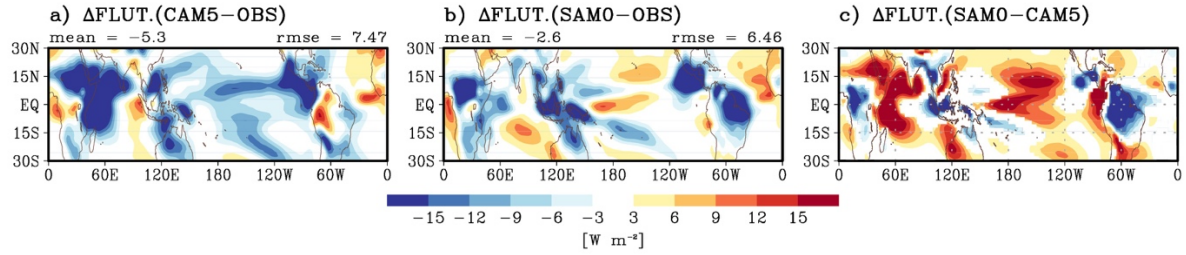

Supplementary Figure S6. biases of annual-mean upward longwave (LW) radiative flux at TOA (FLUT) against the CERES–EBAF observation from (a) CAM5 and (b) SAM0 and (c) difference of FLUT between SAM0 and CAM5. The CERES-EBAF observations were averaged from 2000 to 2013 and the model results are the means of AMIP simulation results for 36 years from January 1979 to February 2015. Shaded areas in (c) exceed a 95 % significance level from the Student t-test.

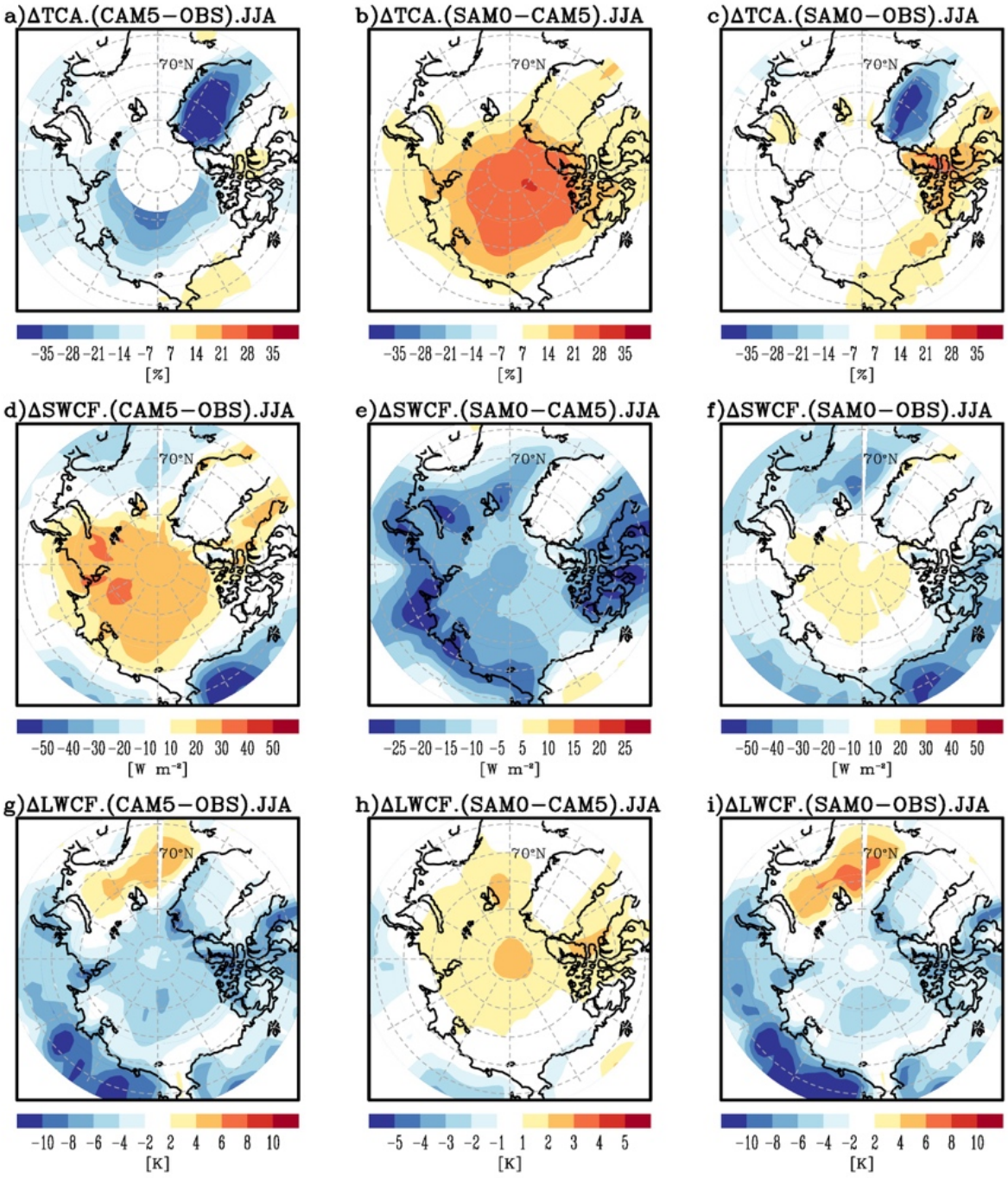

Supplementary Figure S7. Biases of (upper) TCA against the CALIPSO–GOCCP observation, (middle) shortwave cloud forcing at TOA (SWCF) and (lower) longwave cloud forcing at TOA (LWCF) against the CERES–EBAF observation during JJA obtained from (left) CAM5 and (right) SAM0; and (center) differences of each variable between SAM0 and CAM5. The CERES-EBAF observations were averaged from 2000 to 2013, ERA-Interim reanalysis was averaged from January 1979 to February 2015, and the model results are the means of AMIP simulation results for 36 years from January 1979 to February 2015. Shaded areas in (b), (e), and (h) exceed a 95 % significance level from the Student t-test.